Icarus 219 (2012) 630–640

Contents lists available at SciVerse ScienceDirect

Icarus

journal homepage: www.elsevier.com/locate/icarus

Effects of space weathering on diagnostic spectral features: Results from He^+ irradiation experiments

Xiaohui Fu [a,b], Yongliao Zou [a,*], Yongchun Zheng [a], Ziyuan Ouyang [a,c]

[a] National Astronomical Observatories, Chinese Academy of Sciences, Beijing 100012, China
[b] Graduate University of Chinese Academy of Sciences, Beijing 100039, China
[c] Institute of Geochemistry, Chinese Academy of Sciences, Guiyang 550002, China

ARTICLE INFO

Article history:
Received 28 September 2011
Revised 6 March 2012
Accepted 8 March 2012
Available online 24 March 2012

Keywords:
Space weathering
Moon
Asteroids
Solar wind

ABSTRACT

We performed ion irradiation of mineral samples with 50 keV He^+, aimed to investigate ion irradiation effects on diagnostic spectral features. Reflectance spectra of samples in 0.375–2.5 μm are measured before and after ion irradiation. Silicates, including Luobusha olivine, plagioclase and basaltic glass, have shown reddening and darkening of reflectance spectra at the VIS–NIR range. Olivine is more sensitive to ion irradiation than plagioclase and basaltic glass. Irradiated Panzhihua ilmenite exhibits higher reflectance and stronger absorption features, which is totally different from lunar soil and analog silicate materials in other experiments. Using continuum removal and MGM fit, we extracted and compared absorption features of olivine spectra before and after irradiation. Ion irradiation can induce band strength decrease of olivine but negligible band centers shift. We estimate band centers shift caused by ion irradiation are quite limited, even less than variations due to chemical composition in silicates. It provides one possible explanation for no systematic shift in band positions in lunar soil. Irradiated Luobusha olivine spectrum matches spectra of olivine-dominated asteroids. Our results suggest space weathering should be new clues to explain the subtle difference between A-type asteroid spectra and laboratory spectra of olivine.

1. Introduction

Space weathering is the physical and chemical alteration changes at the surface of airless bodies. It includes two main processes: cosmic and solar wind ions irradiation and micrometeorite bombardment. Space weathering was initially studied on lunar soil, since Apollo lunar soils have optical properties that significantly differ from pristine rocks which they were derived (Conel and Nash, 1970; Pieters et al., 1993). With increased weathering, spectra of lunar soils exhibit systematically lower albedos (darken), redder spectral slopes (redden), and weaker mineral absorption features. Pieters et al. (2000) proposed nanophase metallic iron, produced by vapor deposition and irradiation effects, dominates the optical properties of lunar soils. It also has been suggested that space weathering should be responsible for the spectral mismatch between ordinary chondrite and S-type asteroid, which were thought to represent their parent bodies (Chapman, 1996; Pieters et al., 2000).

To interpret spectral modifications on airless bodies by solar wind, simulations have been performed via keV–MeV ion irradiation. Hapke (1973) showed that H^+ irradiation of loose mineral powder visibly darkened the irradiated surface. Dukes et al. (1999) irradiated olivine samples with 1 keV H^+ and 4 keV He^+. By in situ surface analysis, Fe^{2+} near the surface of olivine was reduced into metallic iron. However, no significant spectral changes were detected. Yamada et al. (1999) performed high energy (MeV) proton irradiation on olivine and pyroxene. Only small changes in the spectra were observed, which could be attributed to low irradiation fluence. Different results were obtained by Strazzulla et al. (2005), Brunetto and Strazzulla (2005), and Marchi et al. (2005). They performed ion irradiation of ordinary chondrite (Epinal), minerals (olivine and orthopyroxene), bulk silicate rock with different ions (60–400 keV H^+, He^+, Ar^{2+}). All the irradiated materials have shown darkening and reddening of reflectance spectra in the visible and near-infrared (VNIR) range. Loeffler et al. (2009) observed reddening in NIR reflectance of olivine before and after 4 keV He^+ irradiation. But there is no band center shift for ~1 μm absorption band of olivine.

However, these investigations are far from enough. Firstly, spectral slope (or color index) and albedo are often used as spectral parameters in previous space weathering study, including laboratory simulations. Actually, these are not considered diagnostic parameters for mineralogy because they do not have functional relationships with mineral type, mineral composition, or mineral abundance (Gaffey, 2010). Even though some determined variation

* Corresponding author.
E-mail address: ylzou@bao.ac.cn (Y. Zou).

0019-1035/$ - see front matter © 2012 Elsevier Inc. All rights reserved.
http://dx.doi.org/10.1016/j.icarus.2012.03.009

of band area or BAR values (Band II/Band I area ratio), previous results may not essentially reveal absorption features modifications induced by ion irradiation. Secondly, most of these simulations only focus on mafic minerals, such as olivine and pyroxene, which are the most abundant minerals in ordinary chondrites. But spectral modifications of other mineral during ion irradiation have not been well characterized. This may impede our understanding of diverse space weathering on different types of asteroids.

In the present study, we simulated ion irradiation on minerals and basaltic glass with 50 keV He^+ and measured their reflectance spectra before and after ion irradiation. Absorption band center and strength are regarded as diagnostic parameters since they have a demonstrated functional relationship with mineral type, chemical composition, and mineral abundance (Gaffey, 2010, and references therein). Continuum removal and Modified Gaussian Model (MGM) were employed to extract diagnostic parameters from reflectance spectra. Negligible band center and significant strength decrease due to ion irradiation are recognized.

2. Experiments

2.1. Sample preparation

Terrestrial minerals olivine, plagioclase feldspar, ilmenite and volcanic glass were chose in the experiments. Luobusha olivine ($\sim Fo_{80}$) is picked from the formation of dunites in the Luobusha ophiolite, Southern Tibet. Plagioclase feldspar is from Damiao anorthosite complex. The rocks have experienced different degrees of hydrothermal alteration, such as chloritization (Xie, 1982). Volcanic glass is the most abundant component in lunar soil but has not been involved in previous experiments. Basaltic glass in our study is sampled from Longgang volcanic cluster in northwest of China. Ilmenite is the most common opaque mineral on the Moon (Taylor et al., 1991), as well as possible darkening agent of Mercury's surface (Riner et al., 2009). Panzhihua ilmenite is sampled from Panzhihua ilmenite deposit in south-western Sichuan Province of China.

Major composition of samples was determined by JEOL JXA-8100 electron probe X-ray microanalyzer (EPMA) in Beijing Research Institute of Uranium Geology. The results are listed in Table 1. Luobusha olivine grain size ranges from 400 to 600 μm. Average grain size of plagiolcase and Panzhihua ilmenite is about 200 μm. Basaltic glass grains are between 75 and 100 μm. To prepare our targets, the loose powder sample was packed in aluminum containers and pressed into a pellet under about 300 psi using solid epoxy resin as binder. The epoxy mass fraction in each pellet is no more than 2% to limit the influence on VINIR spectra measurement of the pellets. This organic show no absorptions at the VNIR range, except 1.4 μm band due to hydroxyl band 1.7 μm band due to $CH/CH_2/CH_3$ (Sales et al., 2011). Even though we have not quantified the influence on spectra measurement in this study, the trace binder effects could be neglected here.

2.2. Ion irradiation

He^+ irradiation was performed using LC-4 high energy ion implanter at the Institute of Semiconductors, Chinese Academy of Sciences. The experiments were carried out at room temperature, in an ion pumped ultra-high vacuum (UHV) chamber with residual pressure of 10^{-7} mbar. The energy of ^4He ions is 50 keV. The irradiation fluence is 5×10^{16} ion/cm^2. Beam current density is maintained below 45 μA/cm^2 and ion beam was scanned homogeneously over the target in order to prevent heating during implantation.

The rise in surface temperature of the target during irradiation was not measured. The energy lost by colliding ions is redistributed among the species present in the target, and two main effects occur: displacements of atoms from their lattice position and ionization processes. If assuming 0.1% of energy loss transforms to heat, we estimate the temperature is no higher than 50 °C.

With the SRIM program (at http://www.SRIM.org/, Ziegler et al., 1985), we calculated stopping power and penetration depth in the samples (Table 2). Electronically inelastic processes are found to dominate the collision for 50 keV He^+ implantation in silicates.

2.3. Measurement of reflectance spectra

We measured the reflectance spectra of mineral samples before and after irradiation using Lambda 950 UV/VIS/NIR spectrophotometers at Institute of Remote Sensing Applications, Chinese Academy of Sciences. The reflectance spectra were acquired between 0.375 and 2.50 μm, using a deuterium lamp and a tungsten lamp as radiation sources. The resolution of the spectrophotometer was 1 nm for VNIR range. $BaSO_4$ was taken as a reference for calibration. The measurements were performed in directional–hemi-

Table 1
Major elements concentration (wt.% and standard deviation (1σ)) of Luobusha olivine, plagioclase feldspar, Panzhihua ilmenite and basaltic glass.

Sample	Results (wt.%)										
	SiO_2	TiO_2	Al_2O_3	FeO	MnO	MgO	CaO	Na_2O	K_2O	P_2O_5	Total
Luobusha olivine	40.64	0.01	0.02	11.14	0.14	46.49	0.04	–[a]	–	–	98.48
Plagioclase feldspar	57.85	0.08	25.66	0.24	0.02	0.02	8.02	6.39	0.57	0.03	98.86
Panzhihua ilmenite	–	52.47	–	44.52	0.76	3.33	–	–	–	–	101.08
Basaltic glass	48.84	2.65	13.05	13.62	0.2	8.48	7.81	2.83	1.4	0.25	99.13
Apollo 73,155 glass	46.05	1.69	17.86	9.12	0.124	10.88	10.90	0.629	0.290	–	97.54

[a] Below detection limit. The data of Apollo 73,155 glass are from Tompkins et al. (1996).

Table 2
Stopping power and penetration depth for 50 keV He^+ implantation in silicates.

Sample	He^+ energy (keV)	Ion fluence (He^+/cm^2)	Stopping power (eV/Å)		Penetration depth (Å)
			Inelastic collisions	Elastic collisions	
Luobusha olivine	50	5×10^{16}	10.16	0.324	5600
Plagioclase feldspar	50	5×10^{16}	9.726	0.323	5850
Panzhihua ilmenite	50	5×10^{16}	14.67	0.511	3500
Basaltic glass	50	5×10^{16}	10.98	0.372	4600

spherical reflectance (normal incident) geometry at room temperature and normal atmospheric pressure.

3. Methods

3.1. Continuum removal

The continuum-removal analysis is aimed to isolate major absorption features in the reflectance spectrum. It is a widely used technique by which reflectance spectra are normalized so that comparison can be made of individual absorption features from a common baseline (or continuum) (Clark and Roush, 1984). The continuum $R_c(\lambda_i)$ is a convex hull fit over the top of a spectrum using straight-line segments that connect local spectra maxima. So the continuum removed reflectance $R'(\lambda_i)$ would be calculated as follows:

$$R'(\lambda_i) = R(\lambda_i)/R_c(\lambda_i) \tag{1}$$

$$R_c(\lambda_i) = R_{start} + (R_{end} - R_{start})(\lambda_i - \lambda_{start})/(\lambda_{end} - \lambda_{start}) \tag{2}$$

where $R(\lambda_i)$ is reflectance at the wavelength λ_i, R_{start} and R_{end} represent the reflectances of start point and end point in each straight-line segment, λ_{start} and λ_{end} refer to the wavelengths of start point and end point. Fig. 1 shows the continuum removal by calculating the upper convex hull of a pyroxene spectrum. The continuum removal is implemented in ENVI software package.

3.2. Modified Gaussian Model

The Modified Gaussian Model (MGM) developed by Sunshine et al. (1990), is an inverse model to deconvolve a spectrum into a set of absorptions superimposed onto a continuum slope. Mathematically, the absorptions are defined by Gaussian distributions in average bond length of the site and cation of interest, and in the model are expressed as three parameters for each absorption band: band center, band width, and band strength. The continuum slope is defined by a set of polynomial coefficients, which act as additional model parameters. The model adjusts the various models parameters to minimize, in a least squares sense, the sum of the squares of the residuals.

In MGM, natural log of each reflectance spectrum is modeled as:

$$Ln[R(\lambda)] = C_0 + C_1/\lambda + \sum_{i=1}^{N} s_i \cdot \exp\left[-\frac{(\lambda^{-1} - \mu_i)^2}{2\sigma_i^2}\right] \tag{3}$$

The background continuum component is expressed as:

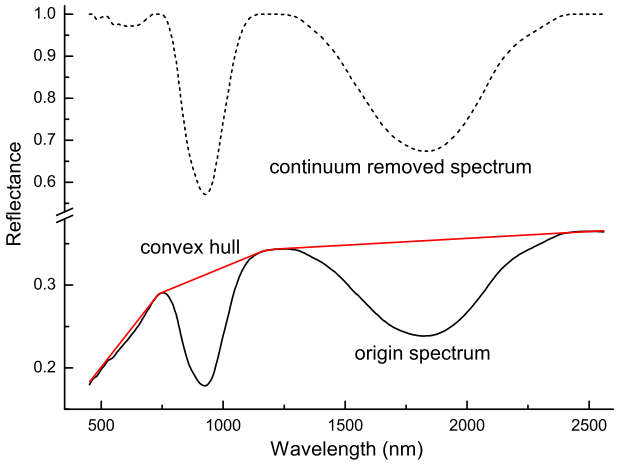

Fig. 1. Example of continuum removal on a pyroxene spectrum.

$$C(\lambda) = C_0 + C_1/\lambda \tag{4}$$

where λ is the wavelength, $R(\lambda)$ reflectance at wavelength λ, s band strength, μ band center, σ band width, N the number of bands. C_0 (continuum slope) and C_1 (the intercept) for the linear function in wavenumber are supposed to be constant parameters. The full width at half maximum (*FWHM*) is calculated by

$$FWHM = 2\sqrt{2\log 2}\cdot\sigma \cong 2.3548\sigma \tag{5}$$

The MGM program is obtained from NASA/Keck Reflectance Experiment Laboratory (RELAB) at Brown University (http://www.planetary.brown.edu/relab/).

4. Results

4.1. Reflectance spectra of ^{4}He irradiated samples

4.1.1. Luobusha olivine

Fig. 2a shows the reflectance spectra of Luobusha olivine before and after He^+ irradiation. Unirradiated Luobusha olivine spectra exhibit a broad, composite absorption feature near 1.05 μm. The absorptions are caused by electronic transitions in Fe^{2+} ions located in distorted octahedral crystallographic sites. The central absorption is caused by Fe^{2+} in the M2 site, while the two exterior absorptions are due to Fe^{2+} in the M1 site (Burns, 1970, 1974, 1993; Burns et al., 1972). Weak absorption bands near 1.9 μm are related with water in the sample while the 2.3 μm absorptions may be due to metal-OH vibrational transitions (Clark, 1999).

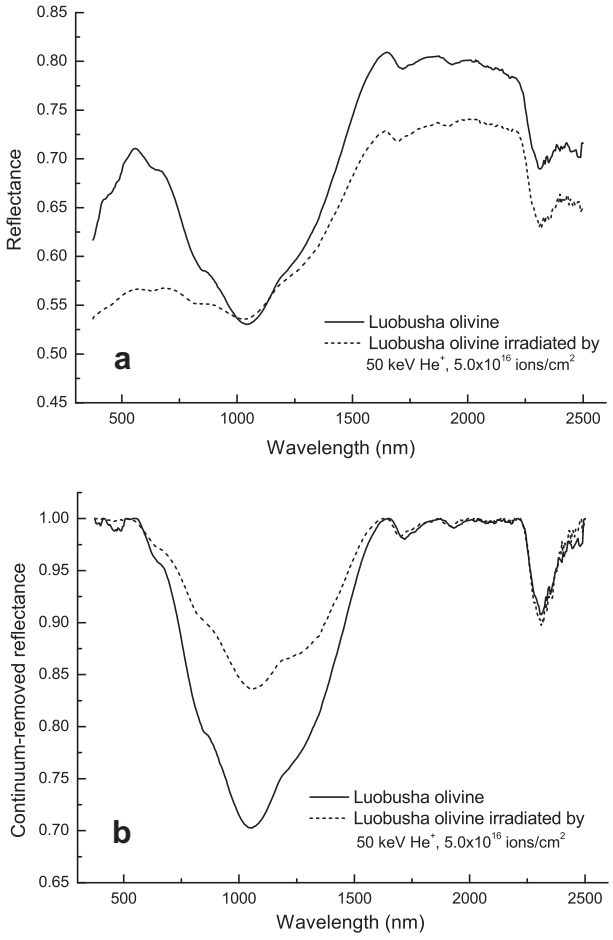

Fig. 2. (a) Origin reflectance spectra of Luobusha olivine before and after He^+ irradiation, and (b) continuum removed spectra of Luobusha olivine.

For irradiated Luobusha olivine, the most obvious spectral change is the drop in overall reflectance. The maximum of the reduction locates at 554 nm. This means He^+ irradiation produced darkening of olivine's reflectance spectra. In addition, olivine became reddening after ion irradiation. We define spectral slope r from reflectance values R as: $r = [R(2.0\ \mu m) - R(0.5\ \mu m)]/1.5\ \mu m$, where 1.5 μm is the difference in wavelength. Spectral slope r of olivine is 0.073 and 0.118, respectively before and after irradiation. The clear slope change shows that He^+ irradiation caused reddening of olivine spectrum. All of these observations are generally consistent with previous experiments (Brunetto and Strazzulla, 2005; Loeffler et al., 2009; Marchi et al., 2005; Strazzulla et al., 2005).

Fig. 2b shows the continuum removed reflectance spectra of Luobusha olivine. Alteration of 1 μm absorption band caused by irradiation was enhanced by this process. Ion irradiation resulted in significant decreasing of band depth and area, which agree with weaker absorption feature of mature lunar soil and analog materials in other experiments. Band center of 1 μm absorption feature shifted towards longer wavelength from 1.040 μm to 1.045 μm. Nevertheless, there are no modifications for other bands at 1.75 μm, 1.9 μm, and 2.3 μm.

4.1.2. Plagioclase feldspar

In remote reflectance analyses, plagioclase is considered to be a weak absorber, almost featureless (Cloutis and Gaffey, 1991). The curve of plagioclase spectra in the study does not look completely similar to lunar anorthite (e.g., LS-CMP-004 in RELAB), which is associated with hydrothermal alteration in our sample. The reflectance show remarkable drop-offs at short wavelength (less than 1.0 μm). We attributed it to chloritization in the feldspar structure. The shallow absorptions at 1.9 μm can be due to the presence of water in the mineral while absorption feature near 2.2 μm are attributed to Al–OH bend vibration, as well as Fe–OH bend (Clark, 1999).

He^+ irradiation induced darkening and reddening of plagioclase spectra (Fig. 3a). The reflectance values obviously decreased after ion irradiation, especially in the visible. Spectra slope r increased from 0.086 to 0.120, which means the spectrum turned redder after irradiation. These results show no difference with mafic mineral in previous investigations (Brunetto and Strazzulla, 2005; Marchi et al., 2005; Loeffler et al., 2009).

Fig. 3b illustrates the continuum removed reflectance spectra of plagioclase. The most notable feature is band center shifted from 1.025 to 0.845 μm. However, this alteration cannot be attributed to ion irradiation. We took straight-line continuum removal in this study, which prevents from properly modeling absorption features that exit at the edge of the wavelength range.

4.1.3. Basaltic glass

Fig. 4a shows spectra of basaltic glass before and after irradiation. This sample exhibits a strong absorption band in the visible range and a broad absorption feature near 1.5 μm. The curve of basaltic glass is similar to that of Apollo 73155 glass samples (Tompkins et al., 1996), but with overall lower reflectance. 73155 glass samples demonstrate a broad absorption band centered just beyond 1 μm and 1.9 μm, due to crystal field transitions of Fe^{2+} in octahedral and tetrahedral coordination respectively (Tompkins et al., 1996). The broad absorption band of present basaltic glass can be the result of those two peaks overlapping. The VIS absorption is due to charge transfer between Fe and Ti (Tompkins and Pieters, 2010). The structure at 2.1–2.2 μm could be the result from metal-OH vibrational transitions introduced by chemical alteration.

He^+ irradiation induced darkening and reddening of basaltic glass spectra (Fig. 4a). After irradiation, reflectance of basaltic glass became lower. Because of more obvious reflectance reduction at the shorter wavelengths, irradiated glass spectrum appears to be redder. Spectra slope r changed from 0.011 to 0.036. These changes

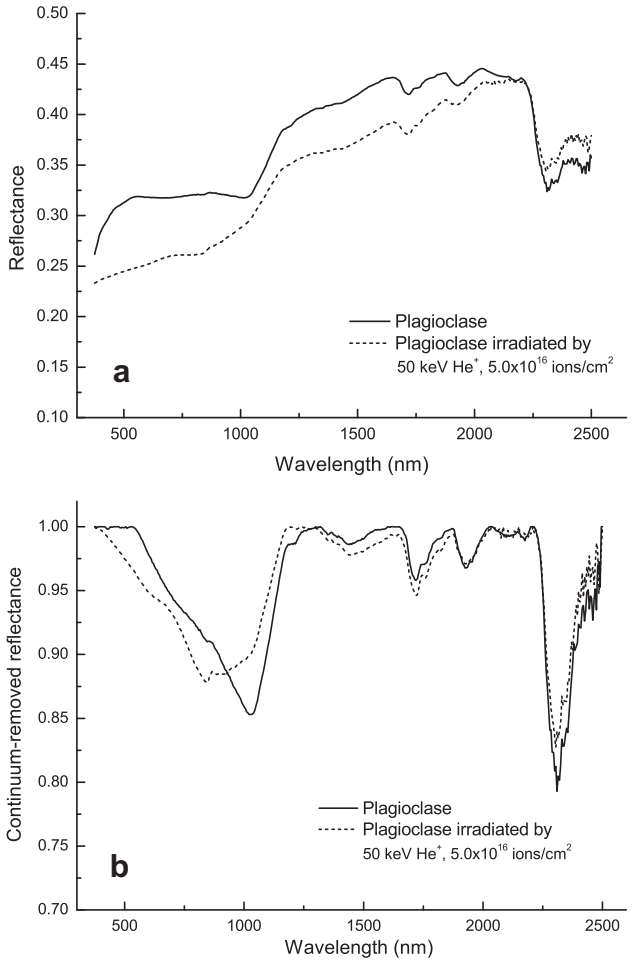

Fig. 3. (a) Origin reflectance spectra of plagioclase before and after He^+ irradiation, and (b) continuum removed spectra of plagioclase.

of glass spectrum before and after irradiation generally are similar to Luobusha olivine and plagioclase described above.

Fig. 4b shows the comparison of continuum removed reflectance spectra before and after ion irradiation of basaltic glass. Note that depth of the absorption band near 1.5 μm became little smaller. However, we cannot determine the band center shift due to irradiation since it is a broad band with no clear peak.

4.1.4. Panzhihua ilmenite

The reflectance spectrum of Panzhihua ilmenite is shown in Fig. 5. The overall reflectance is very low compared with other mineral spectra. The ilmenite spectrum shows the expected broad absorption feature in the ~0.5–0.7 μm region, a local reflectance maximum near 0.8 μm, and a weak broad wavelength absorption band centered near 1.3 μm due to Fe^{2+} ions; reflectance increases shortward of ~0.5 μm, which could be caused by charge transfer. This is because ilmenite is an opaque Fe–Ti oxide mineral, whose optical characteristics are controlled by Fresnel reflection from its surface (Pompilio et al., 2007).

He^+ irradiation dramatically modified spectrum of Panzhihua ilmenite, as shown in Fig. 5. Irradiated ilmenite show stronger absorption features and higher reflectance, which are completely different with what happened to Luobusha olivine and plagioclase, termed darkening and reddening. After irradiation, reflectance of ilmenite increased across the full VNIR range, especially at the wavelength 1.0–1.6 μm and beyond 2.0 μm. Note that absorption band near 1.3 μm becomes deeper and narrower after ion irradia-

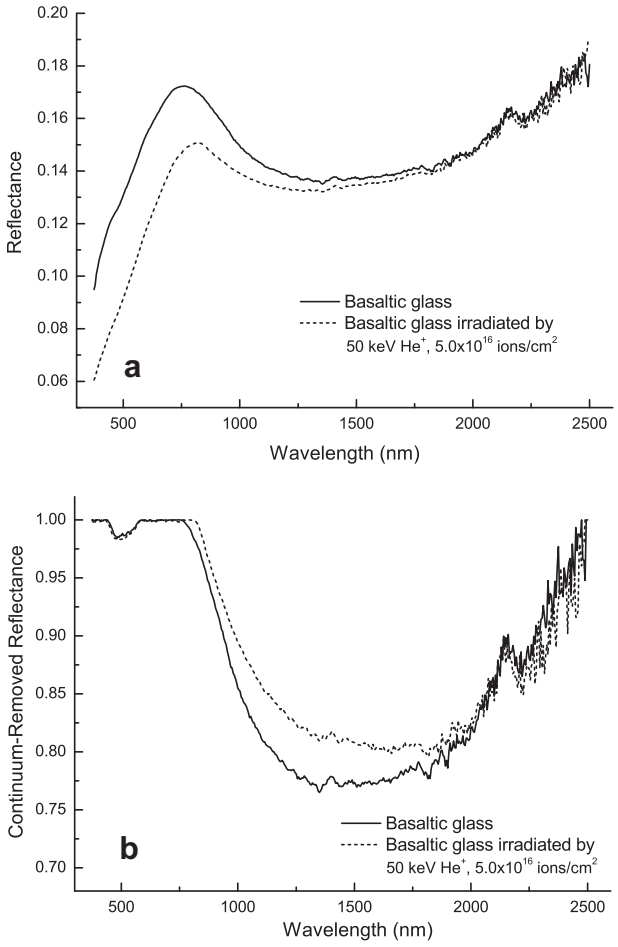

Fig. 4. (a) Origin reflectance spectra of basaltic glass before and after He^+ irradiation, and (b) continuum removed spectra of basaltic glass.

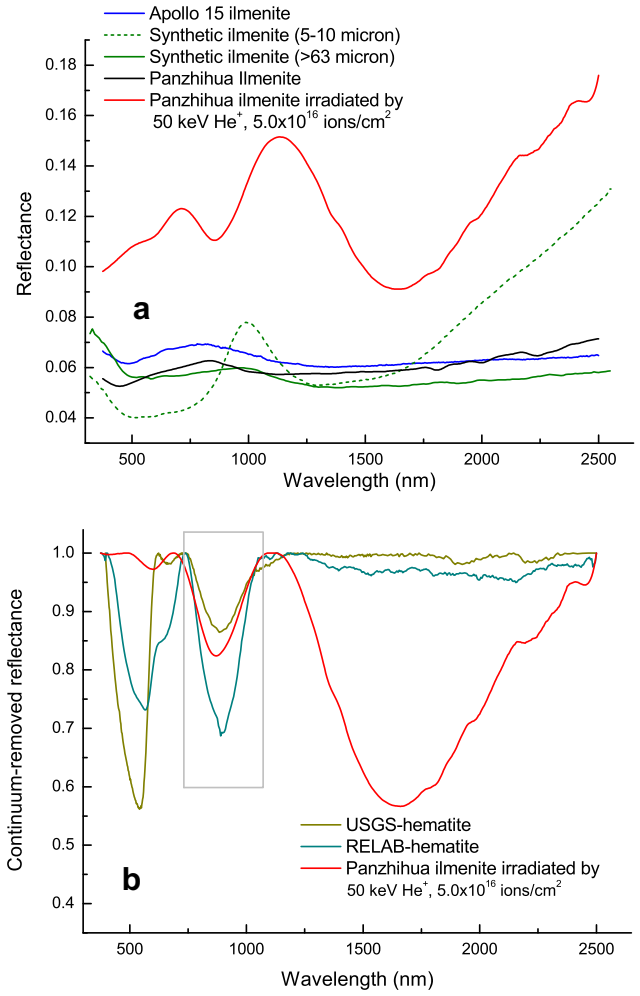

Fig. 5. (a) Origin reflectance spectra of Panzhihua ilmenite and lunar ilmenite, and (b) continuum removed spectra of irradiated Panzhihua ilmenite and hematite. Apollo 15 ilmenite (PI-CMP-006) is from RELAB. The green solid and dash lines represent synthetic ilmenite (5–10 μm) and (size > 63 μm) and spectra data are from RELAB. Hematite data are from RELAB and USGS spectra library. (For interpretation of the references to color in this figure legend, the reader is referred to the web version of this article.)

tion, although we cannot determine how much this band center shifted. Irradiated ilmenite displays a new band near 0.87 μm. This corresponds to the characteristic absorption feature of hematite (α-Fe_2O_3), which is due to Laporte-forbidden transitions (Clark, 1999 and references therein). It implies that He^+ irradiation may induce phase transition in Panzhihua ilmenite. The similar results have been reported by several experiments (Watanabe et al., 1996, 2002; Christoffersen and Keller, 2007; Dai et al., 2007).

As opaque mineral, the reflectance of ilmenite is increasing with decrease grain size (Fig. 5a). Synthetic ilmenite (5–10 nm) shows similar NIR spectrum with irradiated Panzhihua ilmenite but distinct absorption feature in the visible range. Besides, there is no evidence that He^+ irradiation could change grain size distribution of Panzhihua ilmenite. Previous investigations (e.g., Raineri et al., 2000) demonstrate ion irradiation could cause surface roughness increasing, as a result of blister formation and sputtering. The increased surface roughness of ilmenite grain is a possible explanation to brightening of irradiated ilmenite.

4.2. Modified Gaussian Model deconvolutions of olivine spectra

In order to quantify spectral modification due to ion irradiation, we utilized MGM to deconvolve the spectra of Luobusha olivine in this study and San Carlos olivine (Loeffler et al., 2009; Marchi et al., 2005). MGM results are sensitive to the starting parameters. A variation has been noted between MGM calculated absorption center and the real mineralogical absorption center (Kanner et al., 2007; Isaacson et al., 2011). For this study, we first model reflectance spectrum of unirradiated sample. Then, the results, including band center, FWHM and band strength, would be applied as the initial parameters in irradiated spectrum fit. The method could reduce the uncertainties of these parameters. Kanner et al. (2007) performed the sensitivity test to determine an uncertainty on resultant band centers for laboratory meteorite spectra. We estimate error bar of band centers corresponds to ±8 nm for the VNIR range, using the same method of Kanner et al. (2007).

As we talked above, the spectra of samples turned red after irradiation. The ubiquitous but variable nature of continuum slopes in the VNIR reflectance spectra is a major complication in quantitative analysis of diagnostic absorption features. For this study, the increasing slope could introduce an apparent band center shifts to shorter wavelength if we directly use original reflectance spectra in MGM fits. The continuum-removed spectra are adopted in the following MGM fits instead of original reflectance spectra. Because continuum-removal could cause the MGM derived band centers to cluster around nearly identical wavelength (Isaacson et al., 2011).

4.2.1. Luobusha olivine

In the present study, we only focus on 1.0 μm absorption of Luobusha olivine. The results of MGM deconvolutions on continuum-removed spectra of olivine samples are shown in

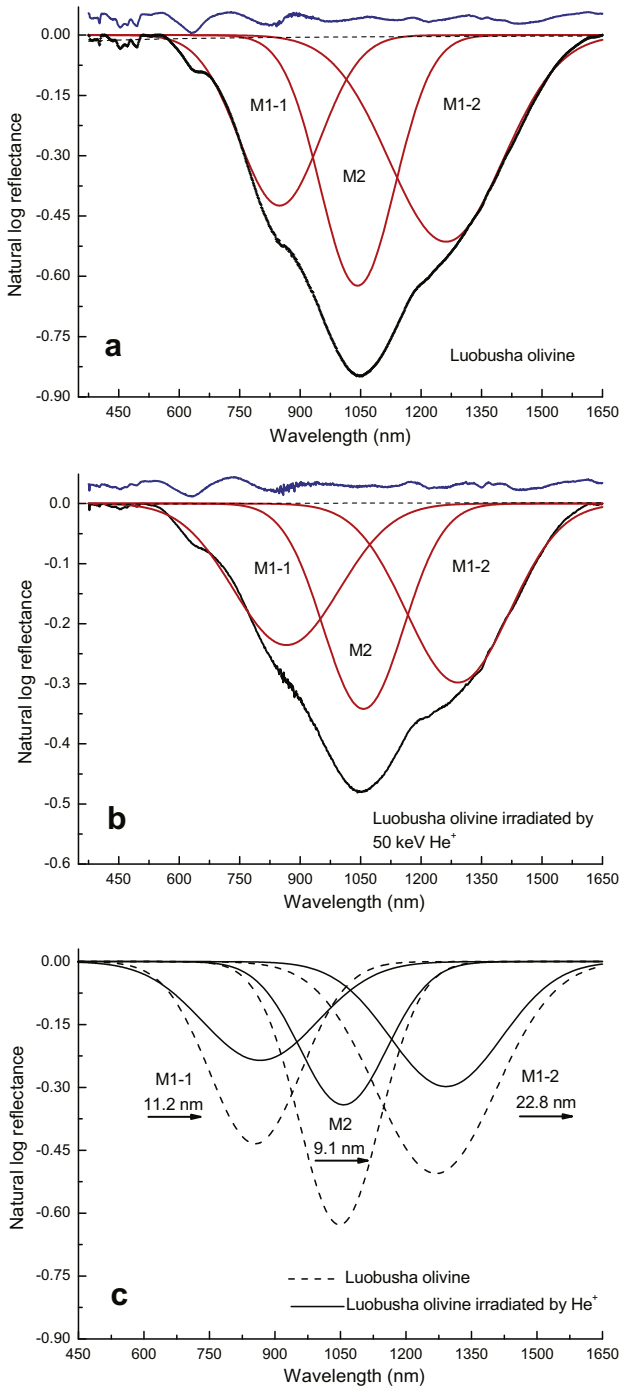

Fig. 6. Modified Gaussian Model fits of origin and irradiated Luobusha olivine. (a) Unirradiated Luobusha olivine sample. (b) Luobusha olivine irradiated by 50 keV He^+, 5×10^{16} ions/cm^2. Natural logarithm reflectance spectrum and modified Gaussians are respectively shown in black and red solid line, and slash line represent the continuum spectrum. Residual error spectrum (blue solid line) is shown in the top of each plot. (c) Absorption bands comparison before and after irradiation. The numbers and arrows show band center variation and shift direction after irradiation. (For interpretation of the references to color in this figure legend, the reader is referred to the web version of this article.)

Fig. 6. Parameters of the deconvolutions of olivine sample are listed in Table 3. Note that band centers all shifted towards longer wavelengths, 11.2 nm, 9.1 nm, and 22.8 nm, individually for M1-1, M2, and M1-2. After irradiation, these individual bands all turned narrower and shallower (Fig. 6c). Bands strength decreased about 43% on the average. In other words, absorption features of irradiated olivine exhibited decreasing strength and width.

4.2.2. San Carlos olivine

Using the same approach, we analyzed the spectra of San Carlos olivine irradiated by 4 keV He^+ (Loeffler et al., 2009) and 200 keV Ar^+ (Marchi et al., 2005). The MGM fits are showed in Fig. 6. Parameters of absorption bands are listed in Table 3. Although there are some spectral discrepancies between two investigators' studies, San Carlos olivine spectra are fitted successfully using the MGM. San Carlos olivine exhibited pronounced decrease in band strength (Fig. 7c and f), just like Luobusha olivine in the present study. However, no systematic shift in band centers occurred up fro irradiated San Carlos olivine. 4 keV He^+ irradiation did not induce wavelength shift at all (Fig. 7c). All the values are even lower than band center uncertainty. For the simulation by Marchi et al. (2005), band center shift due to 200 keV Ar^+ irradiation are not in consistent direction, −3.9 nm, −0.1 nm, +11.8 nm, respectively for M1-1, M2, and M1-2 (Fig. 7f).

5. Discussion

5.1. Different space weathering trends of minerals and diversity of space weathering

Under the same conditions of ion irradiation, different minerals show different sensitivity for space weathering. Compared with previous simulations, we chose more divers minerals in our experiments. Luobusha olivine and plagioclase are both silicate minerals; glass is basaltic silicate without crystal structure. After irradiation, all of them showed lowered albedo, reddish slope and weakened absorption features, just like lunar soil and analog materials in other experiments. However, spectral modifications due to ion irradiation are in various degrees. In the three of them, Luobusha olivine darkened mostly, plagioclase came as the second, and then basaltic glass. Similarly, Ar^+ ion irradiation experiments showed that olivine reddens more efficiently than orthopyroxene (Marchi et al., 2005; Strazzulla et al., 2005; Brunetto et al., 2006a). Besides, laboratory laser experiments showed that the slope changes of pyroxene spectra are much smaller than those of olivine (Sasaki et al., 2002).

Except spectrum slope, we also calculated the C_s values of three silicate samples, space weathering index, which becomes more negative as the space weathering effect increase (Brunetto et al., 2006a). Luobusha olivine ($C_s = -0.038$) shows lower value than plagioclase ($C_s = -0.019$) and basaltic glass ($C_s = -0.008$). The results indicate olivine should be more sensitive to ion irradiation than plagioclase and basaltic glass. All these results confirm that silicate minerals display different sensitivity to ion irradiation and micrometeorite bombardment.

As opaque oxide, Panzhihua ilmenite' spectrum evolved toward distinctive trend during ion irradiation. Long exposure to space may induce more pronounced spectral alteration on airless asteroids than we ever thought. And it may imply a significant amount of a new phase(s) had been produced in irradiated ilmenite. Lunar-style space weathering (Hapke, 2001; Pieters et al., 2000) could not perfectly explain spectral modifications of ilmenite. It has been suggested that the 'redden', 'darken', and weaken absorption feature could not represent spectral evolution trend of different minerals during space weathering process.

The present results imply diversity of space weathering on asteroids. Asteroid surface consists of minerals such as olivine, pyroxene, feldspar, oxide and NiFe metal (Gaffey et al., 2002). In other words, spectrum of each mineral could be taken as the end-member of asteroids spectra. From the discussion above, we conclude minerals may exhibit different sensitivity and trend in space weathering. Therefore, mineralogical characterizations of asteroids play a central role in asteroids' space weathering

Table 3
Parameters of the deconvolutions of Luobusha olivine and San Carlos olivine.

	Band parameter	Luobusha olivine		San Carlos olivine from Loeffler et al. (2009)		San Carlos olivine from Marchi et al. (2005)	
		Unirradiated	Irradiated by 50 keV He^+	Unirradiated	Irradiated by 4 keV He^+	Unirradiated	Irradiated by 200 keV Ar^+
M1-1	Center	854.9	866.1	851.4	852.4	831.5	827.6
	FWHM	246.3	309.4	158.7	152.6	178.3	141.1
	Strength	−0.434	−0.236	−0.104	−0.0787	−0.202	−0.148
M2	Center	1048.0	1057.1	1029.9	1030.6	1022.7	1022.6
	FWHM	218.7	234.4	213.3	211.9	218.1	204.4
	Strength	−0.628	−0.342	−0.296	−0.267	−0.359	−0.385
M1-2	Center	1269.0	1291.8	1250.9	1250.6	1245.2	1257.0
	FWHM	323.7	300.8	328.6	318.8	413.0	377.1
	Strength	−0.506	−0.298	−0.220	−0.194	−0.448	−0.409

Note: Band centers reported in nm; FWHM values in nm. Strength reported as natural log reflectance. The parameters of unirradiated olivine are taken as the inputs for MGM fit of irradiated olivine spectrum.

(Vernazza et al., 2009). It also suggests the diversity of space weathering and multiple weathering mechanisms on different types of asteroids. These conclusions remand us to understand space weathering in a wider vision. 'Redden', 'darken' of spectrum might be not only spectral trend in space weathering, and our investigations should not be impeded by lunar-style model.

5.2. Effects of space weathering on diagnostic spectral parameters

The data indicate ion irradiation can alter band strength decrease of minerals but negligible band center shifts. Mature lunar soil display lowered albedo, reddish slope and weakened absorption features. However, there seems to be no significant effect of space weathering on diagnostic spectral parameters, such as band position and relative band area. Previous simulations suggest ion irradiation (Brunetto and Strazzulla, 2005; Dukes et al., 1999; Marchi et al., 2005; Yamada et al., 1999) and laser ablation (Brunetto et al., 2006b; Hiroi and Sasaki, 2001; Moroz et al., 1996; Sasaki et al., 2001, 2002; Yamada et al., 1999) cannot affect the band position of silicates. Using the MGM fit, we determined band center shifts and strength reductions of spectra of Luobusha olivine irradiated by 50 keV He^+, and San Carlos olivine irradiation by He^+ and Ar^+.

Band strength reduction occurred for spectra of all irradiated olivine. The MGM results of Luobusha olivine and San Carlos olivine illustrates marked band strength decreases. However, band center shifts of olivine due to ion irradiation seem to be negligible. For Luobusha olivine, wavelengths of the three individual bands (M1-1, M2 and M1-2) systematically shifted to longer wavelength (14.4 nm on average) (Fig. 6). But there are no significant band center shifts for San Carlos olivine irradiated by 4 keV He^+. For 200 keV Ar^+ irradiation, the band shifts are not in a consistent direction. These results suggest that ion irradiation could alter absorption band position but within a limited range.

Micrometeorite impacts, the same as ion irradiation, can induce no systematic change in the 1 μm of olivine. The laser experiments, to simulate micrometeorite bombardment, give the exactly same answer. Even if laser irradiation in Moroz et al. (1996) is so great to produce abundant melt glass, band centers shift of partly altered and altered olivine are 4 and 15 nm, which are close with wavelength error. Hiroi and Sasaki (2001) reported the average band shift for all three bands for unaltered San Carlos olivine to that irradiated by 15 mJ laser is 1.58 nm (range = −5.1 to 7.0 nm) (Isaacson et al., 2011).

We estimate band centers shift caused by space weathering could be less than variations due to chemical composition in minerals. Band centers shift of ion and laser irradiated olivine samples are compiled in Fig. 8. In all these results, the greatest shift is + 22.8 nm for M1–2 band of Luobusha olivine irradiated by 50 keV He^+. The value is still significantly less than band position variation due to Fe/Mg in olivine. As shown in Fig. 8, we estimate band shifts for 1 μm olivine absorption caused by space weathering are even less than absorptions shift caused by iron content variation (Sunshine and Pieters, 1998).

5.3. Astronomical implications

As discussed above, space weathering could not affect absorption band centers. This conclusion agrees with lunar soil, and also provides one possible explanation for no systematic shift in band positions in lunar soil with different I_s/FeO (e.g., Taylor et al., 2001; Noble et al., 2006). Amorphous rim and nanophase iron particle, produced by space weathering, could darken and redden the spectra of lunar soil. But they are insufficient to significantly change absorption band positions of the host. Even if band shift did occur with increasing maturity, it would be negligible for lunar soil with different mineral composition and abundance.

In Fig. 9, the spectra of Luobusha olivine before and after ion irradiation are compared with those of seven A-type asteroid from the Bus–DeMeo taxonomy (DeMeo et al., 2009). Asteroids spectra display lower reflectance, steeper spectral slope, and weaker absorption band, which are reproduced by the spectrum of irradiated Luobusha olivine. The subtle difference between A-type asteroid spectra and laboratory spectra of olivine were attributed to changes in temperature (Sunshine et al., 2007). Our results provide new clues to explain spectral variations of A-type asteroid. Irradiated olivine spectrum matches spectra of olivine-dominated asteroids, especially at NIR range. Comparing with temperature effects, space weathering seems induce more significant spectral modifications. For A-type asteroid, space weathering, as an important progress during long exposure to space, should not be ignored.

The spectral modifications on these analogs reveal the different space weathering trends on A-type asteroid. Shown in Fig. 10 are the Band I centers plotted relative to BAR value for three types (A, S and V) asteroids (Bus, 1999; DeMeo et al., 2009). Spectra of irradiated analogs, olivine, ordinary chondrite, and Eucrite meteorite are also plotted in Fig. 10. No matter irradiation energy and fluence, Eifel ordinary chondrites, Bamble Orthopyroxene and Eucrite meteorites all display no significant band center shift but increasing the ratio BII/BI after ion irradiation. Given no band shift, these irradiated analogs develop along the *x*-axis towards increasing BAR value. This indicates S-type and V-type could presumably evolve in the same trend after long exposure to space (Ueda et al., 2002; Pieters et al., 2006). For olivine samples, there are neither band area variation (Band II area = 0) nor significant center shift in the space weathering. Therefore, we interpret olivine-dominated A-type asteroid may display no preferred change directions in this

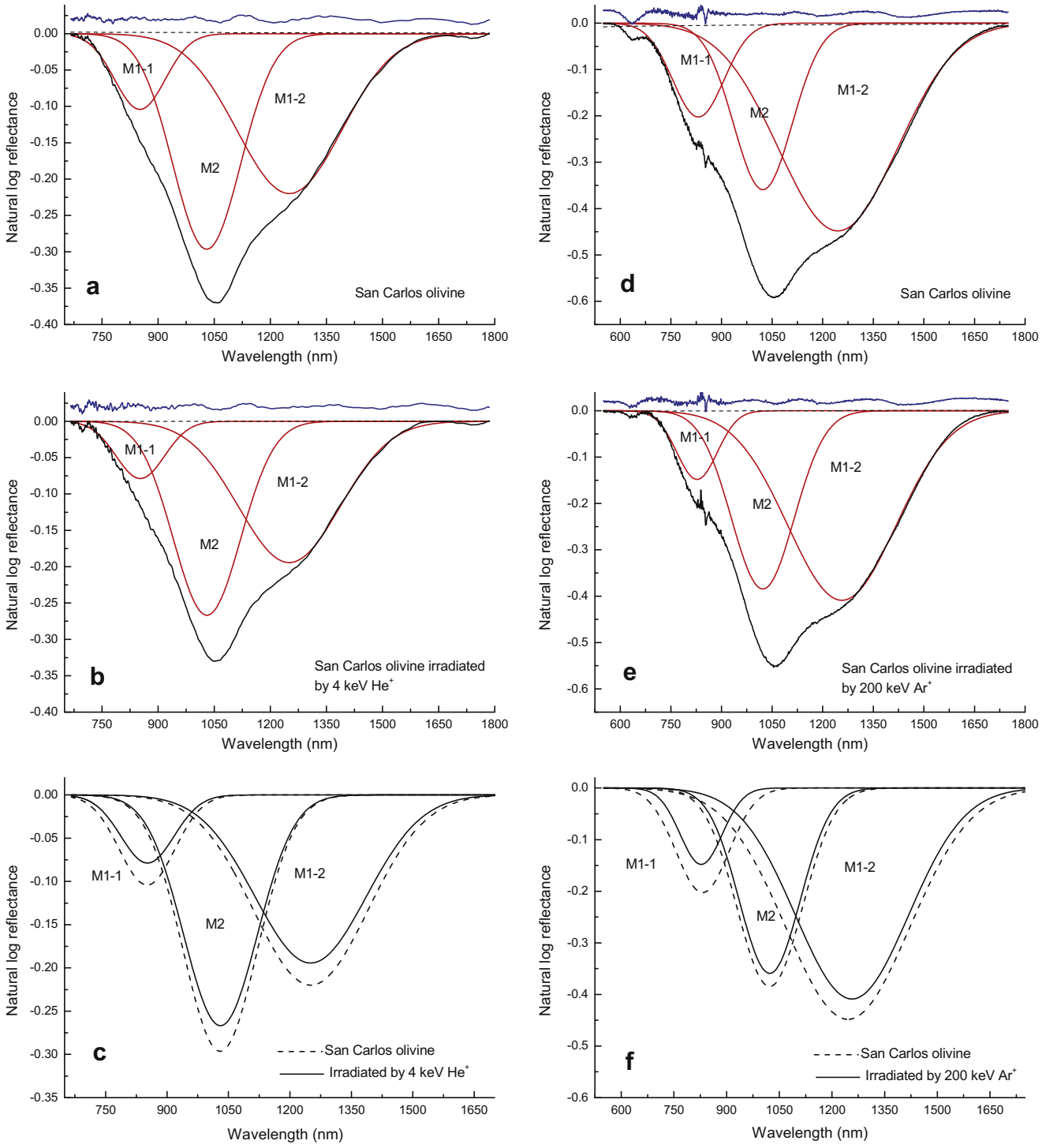

Fig. 7. Modified Gaussian Model fits of San Carlos olivine. (a)–(c) The spectra data of >45 μm olivine are derived from Loeffler et al. (2009). (d)–(f) Olivine (100–200 μm in grain size) spectra data are from Marchi et al. (2005). Natural logarithm reflectance spectrum and modified Gaussians are respectively shown in black and red solid line, and slash line represent the continuum spectrum. Residual error spectrum (blue solid line) is shown in the top of each plot. (For interpretation of the references to color in this figure legend, the reader is referred to the web version of this article.)

OL rectangle of Fig. 10. This inference seems consistent with Main Belt olivine-dominated asteroids (Sunshine et al., 2007). If so, A-type asteroids would evolve in different space weathering trends with S and V types asteroids.

Like the Moon, Mercury has no atmosphere to protect it from the harsh space environment and therefore it is expected that it will also incur the effects of space weathering (e.g. Hapke, 2001). Mariner 10 (Robinson and Lucey, 1997; Denevi and Robinson, 2008) and MESSENGER (McClintock et al., 2008; Robinson et al., 2008; Riner et al., 2009) data reveal one or more opaque components on the Mercury's surface. Ilmenite has been suggested as a candidate mineral of global darkening agent to explain the low albedo. However, irradiated Panzhihua ilmenite shows strong absorptions near 0.87 μm and 1.6 μm. These findings seem to contract the fact that Mercury display absence of identifiable near-infrared absorptions (McClintock et al., 2008). Riner et al. (2009)

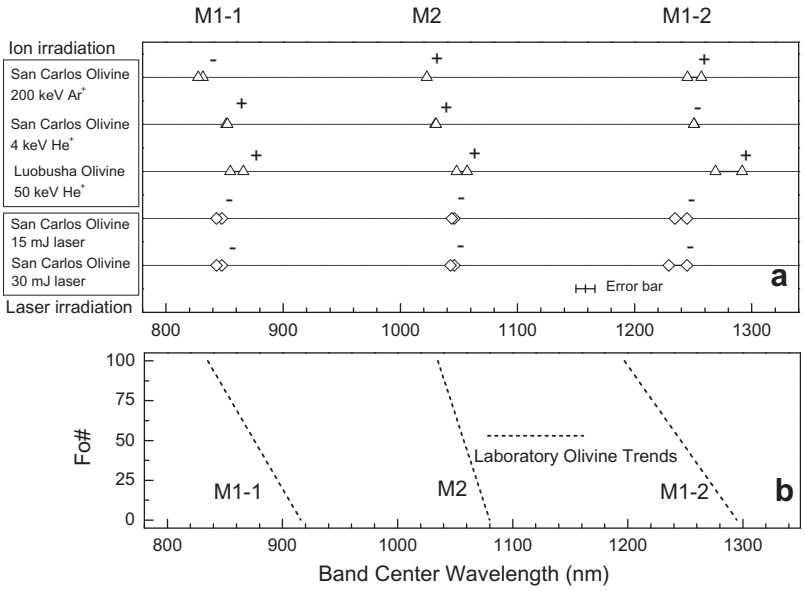

Fig. 8. (a) Comparisons of band centers shift of olivine irradiated by energy ion and laser. Six symbols on each horizontal line represent the three bands of ~1 μm olivine absorption, before and after irradiation. The difference between each symbol and the close one is the value of band center shift. The plus '+' represent band shift toward longer wavelengths while the minus '–' shorter wavelengths. The data of San Carlos Olivine irradiated by 200 keV Ar^+ and 4 keV He^+ are from Marchi et al. (2005) and Loeffler et al. (2009). Laser irradiation data are from Hiroi and Sasaki (2001) and Isaacson et al. (2011). The band centers are determined using the same method as our study. (b) MGM-derived band centers shift of laboratory olivine (Sunshine and Pieters, 1998).

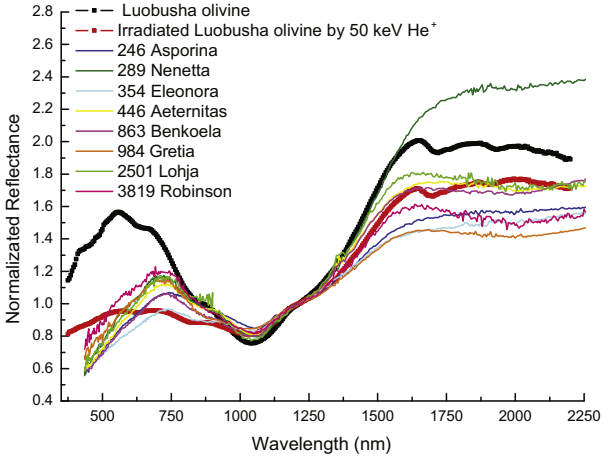

Fig. 9. Comparison of Luobusha olivine reflectance spectra before and after irradiation with A-type asteroid spectra. Visible spectra of asteroids are obtained during the Phase II Small Main-belt Asteroid Spectroscopic Survey (SMASS II) program. Near-infrared spectra of asteroids are obtained with SpeX at the NASA Infrared Telescope Facility (IRTF). The reflectance value is normalized to 1 at 1.215 μm.

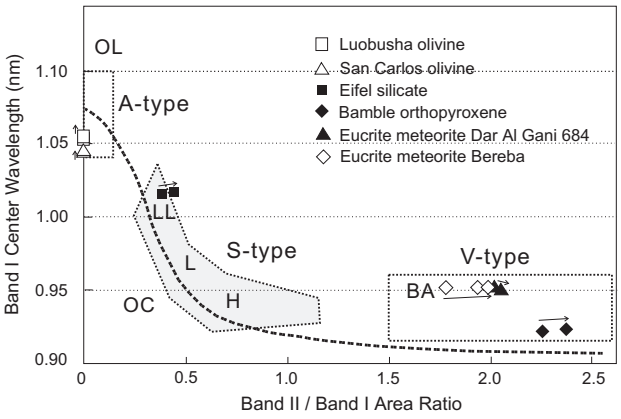

Fig. 10. Plot of Band I center versus Band II/Band I area ratio for A, S and V type asteroids and three types of meteorite assemblages (modified from Gaffey et al. (1993)). OL in the plot is olivine; LL, L and H are three subtypes of ordinary chondrites (OC); BA represents basaltic achondrite. The arrows show the changes directions due to space weathering. San Carlos olivine, Eifel silicate and Bamble Orthopyroxene data are from Marchi et al. (2005). Eucrite meteorite Dar Al Gani 684 and Bereba are from Fulvio et al. (2012). Irradiation conditions are listed in the references.

excluded Fe, Ti-bearing oxides because other payloads results suggest a low TiO_2 abundance on Mercury's surface. Except ilmenite, there are other opaque mineral on Moon, Mercury and asteroids, such as spinel and rutile. Compared with silicates, they exhibit different modifications in space weathering. Clearly, more works about opaque minerals are necessary in future to constrain nature of the darkening agent on Mercury and completely reveal space weathering effects on airless bodies.

6. Conclusions

We performed 50 keV He^+ irradiation on silicate minerals and basaltic glass to simulate ion irradiation in space. This study has allowed us to reach the following conclusions:

(1) Silicates, including Luobusha olivine, plagioclase and basaltic glass, have shown reddening and darkening of reflectance spectra in 0.375–2.5 μm. Olivine is more sensitive to ion irradiation than plagioclase and basaltic glass. Panzhihua ilmenite exhibited higher reflectance and stronger absorption features, which is totally different from lunar soil and analog materials in other experiments. The different weathering trends of mineral indicate diversity space weathering on asteroids.

(2) Using continuum removal and MGM fit, we extracted and compared absorption features of olivine spectra before and after irradiation. Ion irradiation can alter band strength decrease of minerals but negligible band centers shift. We estimate band centers shift caused by ion irradiation are

quite limited, even less than variations due to chemical composition in silicates. It provides one possible explanation for no systematic shift in band positions in lunar soil with different I_s/FeO.

(3) Irradiated Luobusha olivine spectrum can match spectra of olivine-dominated asteroids. Our results suggest space weathering should be new clues to explain the subtle difference between A-type asteroid spectra and laboratory spectra of olivine.

Acknowledgments

This study was supported by The National High Technology Research and Development Program of China (863 Program) (No. 2010AA122200), and the National Natural Science Foundation of China (No. 40904051). The authors appreciate Xirong Yang and Jianming Li for assistance with ion irradiation and spectral measurement. We are grateful to Simone Marchi whose thorough comments and suggestions improve the manuscript. Thanks to Rosario Brunetto and another anonymous referee for their many constructive improvements. We acknowledge the support of RELAB and the access to MGM program and spectra data.

References

Brunetto, R., Strazzulla, G., 2005. Elastic collisions in ion irradiation experiments: A mechanism for space weathering of silicates. Icarus 179, 265–273.

Brunetto, R., Vernazza, P., Marchi, S., Birlan, M., Fulchignoni, M., Orofino, V., Strazzulla, G., 2006a. Modeling asteroid surfaces from observations and irradiation experiments: The case of 832 karin. Icarus 184, 327–337.

Brunetto, R., Romano, F., Blanco, A., Fonti, S., Martino, M., Orofino, V., Verrienti, C., 2006b. Space weathering of silicates simulated by nanosecond pulse UV excimer laser. Icarus 180, 546–554.

Burns, R., 1970. Crystal field spectra and evidence of cation ordering in olivine minerals. Am. Mineral. 55, 1608–1632.

Burns, R., 1974. The polarized spectra of iron in silicates: Olivine. A discussion of neglected contributions from Fe^{2+} ions in M(1) sites. Am. Mineral. 59, 625–629.

Burns, R.G., 1993. Mineralogical Applications of Crystal Field Theory. Cambridge University Press, Cambridge.

Burns, R.G., Huggins, F.E., Abu-Eid, R.M., 1972. Polarized absorption spectra of single crystals of lunar pyroxenes and olivines. Moon 4, 93–102.

Bus, S.J., 1999. Compositional Structure in the Asteroids Belt: Results of a Spectroscopic Survey. Ph.D. Thesis.

Chapman, C.R., 1996. S-type asteroids, ordinary chondrites, and space weathering: The evidence from Galileo's fly-bys of gaspra and ida. Meteorit. Planet. Sci. 31, 699–725.

Christoffersen, R., Keller, L.P., 2007. Space plasma ion processing of ilmenite in the lunar soil: Insights from in situ tem ion irradiation experiments. Proc. Lunar Planet. Sci. Conf. 38, 1969.

Clark, R.N., Roush, T.L., 1984. Reflectance spectroscopy: Quantitative analysis techniques for remote sensing applications. J. Geophys. Res. 89, 6329–6340.

Clark, R., 1999. Spectroscopy of rocks and minerals, and principles of spectroscopy. Manual Remote Sensing 3, 3–58.

Cloutis, E.A., Gaffey, M.J., 1991. Pyroxene spectroscopy revisited: Spectral–compositional correlations and relationship to geothermometry. J. Geophys. Res. 96, 22809–22826.

Conel, J.E., Nash, D.B., 1970. Spectral reflectance and albedo of Apollo 11 lunar samples: Effects of irradiation and vitrification and comparison with telescopic observations. Geochim. Cosmochim. Acta. 1, 2013.

Dai, Y., Guo, X., Zhang, J., 2007. Microstructure changes in the reduction of ilmenite to iron. J. Univ. Sci. Technol. Beijing 29, 373–376.

Demeo, F.E., Binzel, R.P., Slivan, S., Bus, S.J., 2009. An extension of the Bus asteroid taxonomy into the near-infrared. Icarus 2002, 160–180.

Denevi, B.W., Robinson, M.S., 2008. Mercury's albedo from mariner 10: Implications for the presence of ferrous iron. Icarus 197, 239–246.

Dukes, C.A., Baragiola, R.A., McFadden, L.A., 1999. Surface modification of olivine by H^+ and He^+ bombardment. J. Geophys. Res. 104, 1865–1872.

Fulvio, D., Brunetto, R., Vernazza, P., Strazzula, G., 2012. Space weathering of Vesta and V-type asteroids: New irradiation experiments on HED meteorites. Astron. Astrophys. 537, 1–5.

Gaffey, M., Bell, J., Brown, R., Burbine, T., Piatek, J., Reed, K., Chaky, D., 1993. Mineralogical variations within the s-type asteroid class. Icarus 106, 573–602.

Gaffey, M., Cloutis, E., Kelley, M., Reed, K., 2002. Mineralogy of asteroids. In: Bottke, W., Cellino, A., Paolicchi, P., Binzel, R.P. (Eds.), Asteroids III. University of Arizona Press, Tucson, pp. 183–204.

Gaffey, M.J., 2010. Space weathering and the interpretation of asteroid reflectance spectra. Icarus 209, 564–574.

Hapke, B., 1973. Darkening of silicate rock powders by solar wind sputtering. Earth Moon Planets 7, 342–355.

Hapke, B., 2001. Space weathering from Mercury to the asteroid belt. J. Geophys. Res. 106, 10039–10073.

Hiroi, T., Sasaki, S., 2001. Importance of space weathering simulation products in compositional modeling of asteroids: 349 Dembowska and 446 Aeternitas as examples. Meteorit. Planet. Sci. 36, 1587–1596.

Isaacson, P.J. et al., 2011. Remote compositional analysis of lunar olivine-rich lithologies with Moon mineralogy mapper (M^3) spectra. J. Geophys. Res. 116, E00G11.

Kanner, L.C., Mustard, J.F., Gendrin, A., 2007. Assessing the limits of the Modified Gaussian Model for remote spectroscopic studies of pyroxenes on Mars. Icarus 187, 442–456.

Loeffler, M.J., Dukes, C.A., Baragiola, R.A., 2009. Irradiation of olivine by 4 keV He^+: Simulation of space weathering by the solar wind. J. Geophys. Res., 114.

Marchi, S., Brunetto, R., Magrin, S., Lazzarin, M., Gandolfi, D., 2005. Space weathering of near-Earth and main belt silicate-rich asteroids: Observations and ion irradiation experiments. Astron. Astrophys. 443, 769–775.

McClintock, W.E. et al., 2008. Spectroscopic observations of Mercury's surface reflectance during messenger's first Mercury flyby. Science 321, 62–65.

Moroz, L., Fisenko, A., Semjonova, L., Pieters, C., Korotaeva, N., 1996. Optical effects of regolith processes on S-asteroids as simulated by laser shots on ordinary chondrite and other mafic materials. Icarus 122, 366–382.

Noble, S.K., Pieters, C.M., Hiroi, T., Taylor, L.A., 2006. Using the Modified Gaussian Model to extract quantitative data from lunar soils. J. Geophys. Res. 111, E11009.

Pieters, C.M., et al., 2006. Asteroid–meteorite links: The vesta conundrum(s). In: Daniela, L. (Ed.), Asteroids, Comets, Meteors, vol. 229, pp. 273–288.

Pieters, C.M., Fischer, E.M., Rode, O., Basu, A., 1993. Optical effects of space weathering: The role of the finest fraction. J. Geophys. Res. 98, 20817–20824.

Pieters, C.M. et al., 2000. Space weathering on airless bodies: Resolving a mystery with lunar samples. Meteorit. Planet. Sci. 35, 1101–1107.

Pompilio, L., Sgavetti, M., Pedrazzi, G., 2007. Visible and near-infrared reflectance spectroscopy of pyroxene-bearing rocks: New constraints for understanding planetary surface compositions. J. Geophys. Res. 112, E01004.

Raineri, V., Saggio, M., Rimini, E., 2000. Voids in silicon by He implantation: From basic to applications. J. Mater. Res. 15 (7), 1449–1477.

Riner, M.A., Lucey, P.G., Desch, S.J., McCubbin, F.M., 2009. Nature of opaque components on Mercury: Insights into a mercurian magma ocean. Geophys. Res. Lett. 36, L02201.

Robinson, M.S., Lucey, P.G., 1997. Recalibrated mariner 10 color mosaics: Implications for mercurian volcanism. Science 275, 197–200.

Robinson, M.S. et al., 2008. Reflectance and color variations on Mercury: Regolith processes and compositional heterogeneity. Science 321, 66–69.

Sales, R., Diniz, M., Dutra, R., Thim, G., Dibbern-Brunelli, D., 2011. Study of curing process of glass fiber and epoxy resin composite by FT-NIR, photoacoustic spectroscopy and luminescence spectroscopy. J. Mater. Sci. 46, 1814–1823.

Sasaki, S., Hiroi, T., Nakamura, K., Hamabe, Y., Kurahashi, E., Yamada, M., 2002. Simulation of space weathering by nanosecond pulse laser heating: Dependence on mineral composition, weathering trend of asteroids and discovery of nanophase iron particles. Adv. Space Res. 29, 783–788.

Sasaki, S., Nakamura, K., Hamabe, Y., Kurahashi, E., Hiroi, T., 2001. Production of iron nanoparticles by laser irradiation in a simulation of lunar-like space weathering. Nature 410, 555–557.

Strazzulla, G., Dotto, E., Binzel, R., Brunetto, R., Barucci, M.A., Blanco, A., Orofino, V., 2005. Spectral alteration of the meteorite Epinal (H5) induced by heavy ion irradiation: A simulation of space weathering effects on near-Earth asteroids. Icarus 174, 31–35.

Sunshine, J.M., Bus, S.J., Corrigan, C.M., McCoy, T.J., Burbine, T.H., 2007. Olivine-dominated asteroids and meteorites: Distinguishing nebular and igneous histories. Meteorit. Planet. Sci. 42, 155–170.

Sunshine, J.M., Pieters, C.M., 1998. Determining the composition of olivine from reflectance spectroscopy. J. Geophys. Res. 103, 13675–13688.

Sunshine, J.M., Pieters, C.M., Pratt, S.F., 1990. Deconvolution of mineral absorption bands: An improved approach. J. Geophys. Res. 95, 6955–6966.

Taylor, G., Warren, P., Ryder, G., Delano, J., Pieters, C., Lofgren, G., 1991. Lunar rocks. In: Heiken, G., Vaniman, D., French, B.M. (Eds.), Lunar sourcebook: A user's guide to the Moon. Cambridge University Press, Cambridge, pp. 183–284.

Taylor, L.A. et al., 2001. The effects of space weathering on Apollo 17 mare soils: Petrographic and chemical characterization. Meteorit. Planet. Sci. 36, 285–299.

Tompkins, S., Pieters, C.M., 2010. Spectral characteristics of lunar impact melts and inferred mineralogy. Meteorit. Planet. Sci. 45, 1152–1169.

Tompkins, S., Pieters, C.M., Ryder, G., 1996. Spectral variations among crystalline and glassy Apollo 17 impact melt rocks. Proc. Lunar Planet. Sci. Conf. 27, 1335.

Ueda, Y., Hiroi, T., Pieters, C.M., Miyamoto, M., 2002. Changes of Band I center and Band II/Band I area ratio in reflectance spectra of olivine–pyroxene mixtures due to the space weathering and grain size effects. Lunar Planet. Sci. Abstract 2023.

Vernazza, P., Binzel, R.P., Rossi, A., Fulchignoni, M., Birlan, M., 2009. Solar wind as the origin of rapid reddening of asteroid surfaces. Nature 458, 993–995.

Watanabe, Y., Ishii, K., Ishikawa, N., Furuya, K., Kato, M., 2002. In situ observation of transformation in α-Fe_2O_3 under hydrogen implantation. J. Phys. Condens. Mater. 14, 13643–13651.

Watanabe, Y., Takemura, S., Kashiwaya, Y., Ishii, K., 1996. Reduction of haematite to magnetite induced by hydrogen ion implantation. J. Phys. D: Appl. Phys. 29, 8–13.

Xie, G., 1982. Petrological characteristics of the damiao anorthosite complex in Hebei Province, China. Chin. J. Geochem. 1, 369–386.

Yamada, M. et al., 1999. Simulation of space weathering of planet-forming materials: Nanosecond pulse laser irradiation and proton implantation on olivine and pyroxene samples. Earth Planets Space 51, 1255–1265.

Ziegler, J., Biersack, J., Littmark, U., 1985. The Stopping Power and Range of Ions in Solids. Pergamon, New York.